

Estimates of surface drifter trajectories in the equatorial Atlantic: a multi-model ensemble approach

Robert Bruce Scott · Nicolas Ferry · Marie Dréville · Charlie N. Barron ·
Nicolas C. Jourdain · Jean-Michel Lellouche · Edward Joseph Metzger ·
Marie-Hélène Rio · Ole Martin Smedstad

Received: 20 September 2011 / Accepted: 19 April 2012 / Published online: 27 May 2012
© Springer-Verlag 2012

Abstract We compared the estimates of surface drifter trajectories from 1 to 7 days in the equatorial Atlantic over an 18-month period with five eddy ocean general circulation model (OGCM) reanalyses and one

observational product. The cumulative distribution of trajectory error was estimated using over 7,000 days of drifter trajectories. The observational product had smaller errors than any of the individual OGCM reanalyses. Three strategies for improving trajectory estimates using the ensemble of five operational ocean analysis and forecasting products were explored: two methods using a multi-model ensemble estimate and also spatial low-pass filtering. The results were insensitive to the method used to create the ensemble estimates, and by most measures, the results were better than the observational product. Comparison of relative skill of the various OGCM reanalyses suggested promising avenues for exploration for further improvements: forcing with higher frequency wind stress and quality control of input data. One of the lowest horizontal resolution OGCMs, with $1/4^\circ$ longitude horizontal resolution, made the best trajectory estimates. The individual OGCMs were dominated by errors at spatial scales smaller than about 100 to 200 km, i.e., less than the local deformation radius. But buried in those errors were valuable signals that could be retrieved by combining all the OGCM velocity fields to produce a multi-model ensemble-based estimate. This estimate had skill down to spatial scales about 75 km. Results from this study are consistent with previous work showing that ensemble-mean forecast skill is superior to individual forecasts.

Responsible Editor: Oyvind Breivik

This article is part of the Topical Collection on *Advances in Search and Rescue at Sea*

R. B. Scott (✉)
Institute for Geophysics, Jackson School of Geosciences,
The University of Texas at Austin, J.J. Pickle Research
Campus, Bldg. 196 (ROC), 10100 Burnet Rd. (R2200),
Austin, TX 78758, USA
e-mail: robert.scott@univ-brest.fr

R. B. Scott
Laboratoire de Physique des Océans UMR6523
(CNRS, UBO, IFREMER, IRD), Brest, France

C. N. Barron · E. Joseph Metzger
Naval Research Laboratory, Stennis Space Center,
Hancock County, MS 39529, USA

N. Ferry · M. Dréville · J. -M. Lellouche
Mercator-Océan, Toulouse, France

N. C. Jourdain
Laboratoire des écoulements géophysiques et industriels,
Grenoble, France

M.-H. Rio
Collecte Localisation Satellites, Ramonville St-Agne, France

O. M. Smedstad
QinetiQ North America, Stennis Space Center,
Hancock County, MS 39529, USA

Keywords Ocean prediction · Surface drifters ·
Data assimilation · Eddy OGCM ·
Model intercomparison · Model–data comparison ·
Multi-model ensemble prediction

1 Introduction

The problem of predicting or estimating trajectories of objects floating near the sea surface arises in important applications, such as search and rescue missions when something or someone is lost at sea at a known place and time, or when debris from an accident is found and one wishes to find the accident location by integrating back in time the trajectories of the debris. These problems require knowledge of the near surface ocean currents and, to an extent depending upon the floating object, the direct effect of the winds. Here we focus on the first requirement of accurate near surface currents by assessing the predictability of the trajectories of Atlantic Oceanographic and Meteorological Laboratory (AOML) surface drifters drogued at 15 m depth. We focus on the equatorial Atlantic since this is an especially challenging area due to the presence of strong currents having a large space and time variability. This region also corresponds to the area where AF447 flight crashed (close to 3° N, 31° W) 1st June 2009. Several research laboratories and private companies were solicited at that time to provide estimates of the crash position given the location of the recovered debris. Using ocean currents estimates, the backward trajectory hindcast of these floating objects would be a way to estimate the crash location (Dréville et al., this issue). This was a good motivation to study surface drifter trajectories in that region.

In the last few years, operational oceanography centres have developed global forecast, nowcast and hindcast systems providing high spatial resolution ocean currents at daily or higher frequency. These data are used for search and rescue and object drift applications (Davidson et al. 2009) as well as marine oil pollution prediction (Hackett et al. 2009). Only operational ocean analysis and forecasting systems are able to predict with some skill the ocean surface currents, especially when the ocean dynamics is dominated by eddy variability. So it has become an important issue to assess not only surface current Eulerian statistics but also to validate the Lagrangian properties of the ocean circulation in ocean models. The capability of a model to forecast a drifter trajectory is related to the statistics of the distance separating two particles initially close to each other. One expects that with increasing time, this distance will increase according to the dynamics of the ocean circulation. The study of the separation distance between two particles was first addressed by Richardson (1926). In his pioneering study, Richardson proposed that the mean squared separation distance

$\langle d^2 \rangle$ between two particles is proportional to t^3 (t is the time). This behaviour persists until d exceeds the size of the largest eddies and then the separation evolves like a random walk process and $\langle d^2 \rangle$ becomes proportional to time. Thanks to quasigeostrophic turbulence and surface quasigeostrophic turbulence theories, it has been possible to predict the relative dispersion laws as a function of the slope of the kinetic energy wave number spectrum (Sawford 2001; LaCasce 2008). Numerous studies have tried to verify these theories against observations, i.e. balloon (in the atmosphere) or drifter (in the ocean) trajectories. LaCasce (2010) reviews the theoretical probability density functions (PDFs) used to characterize pair separations and tries to assess their validity against PDFs deduced from observations. However, pair separation PDFs are difficult to validate against observations as the samples considered are often small. Results also seem to be sensitive to the region studied as noted by LaCasce (2008) and Lumpkin and Elipot (2010). This is due to the spatial variability of the velocity wave number spectrum. Lagrangian trajectories are in most cases isotropic. However, in some areas, particle separation may be affected by large-scale mean shear. In the case of a zonal front, the meridional separation distance will be different from the zonal one (LaCasce 2008). Particles can also be affected by ocean topography (LaCasce 2008) with trajectories tending to follow f/H contours, with f the Coriolis parameter and H the ocean depth. Modelling studies have investigated the sensitivity of trajectory forecasts to several parameters. Özgökmen et al. (2000) have shown that given sufficient surface drifter coverage, RMS forecast errors of less than 50 km can be obtained for periods up to 3 months in the gyre interior region but only about 1 week in western boundary current and midlatitude jet regions. Their study also shows that the forecast error is very sensitive to the number of observations available to constrain the ocean state during the analysis. In an idealized modelling study, Griffa et al. (2004) revealed that the spatial smoothing of Eulerian fields can reduce the trajectory forecast skill. Thanks to the availability of ocean operational forecasting systems, studies have tried to estimate float trajectory forecast skill in a realistic framework. For example, Barron et al. (2007) assessed surface drifter trajectory estimates in many regions with the global Navy Coastal Ocean Model (NCOM) model. More recently, Huntley et al. (2011) considered trajectory predictions with the US Navy East Asian Sea (EAS16) model and a unique set of 30 surface drifters. It allowed them to show

Table 1 Models analysed in this study

Quantity	GLORYS	PSY3	PSY2	NCOM	HYCOM	SURCOUF
Eqns	PE	PE	PE	PE	PE	G, Ek
Mixing	TKE	TKE	TKE	MY2	KPP	
Vert. co.	Z	Z	Z	Z, σ	ρ, Z, σ	n/a
Nz	50	50	50	40	(32)	1
dz (m)	2.25	2.25	2.25	3.4	2.4	n/a
dx (deg)	1/4	1/4	1/12	1/6	1/12.5	1/3
Wind	EC24	EC24	EC24	NG3	NG3	ERA
Output	Daily mean	Daily mean	Daily mean	6-hourly snapshot	Daily snapshot	6-hourly mean

TKE is Blanke and Delecluse’s (1993) mixed layer scheme; MY2 is Mellor and Yamada’s (1974) mixed layer scheme; KPP is the mixed layer scheme of Large et al. (1994)

PE primitive equations, G geostrophy, Ek Ekman, Nz total number of levels (layers), dz vertical resolution at 15 m, dx horizontal resolution in degree longitude, EC24 daily ECMWF stress, ERA six-hourly ERA Interim stress, NG3 three-hourly NOGAPS

that predictive skill depended more upon deployment location than time of deployment. See Huntley et al. (2011, and references therein) for a summary of several other related studies.

Several questions arise in using operational ocean forecasting systems to estimate drifter trajectories in the real ocean. How reliable are trajectory forecasts made in a realistic framework? Are the forecasts very sensitive to the choice of the operational surface currents used? Do all forecasts have the same skill or are there differences due to model resolution, data assimilation schemes used or observations assimilated? Given an ensemble ocean operational forecasting system, what is the best strategy to perform the most accurate

trajectory forecast? In seeking the best estimate, should one use only the most accurate model? Or is the optimal estimate obtained by combining the estimates from some or all of the models? How should one combine the model estimates: by combining their velocity fields and performing the integration with the compromise velocity, or by performing each model integration separately and combining their estimated trajectory end points? We addressed these questions rigorously by assessing drifter trajectory estimate success using products summarized in Table 1 and described in more detail in the “Appendix” and in Tables 2 and 3.

Most of the models are based upon primitive equation, global or basin scale, ocean general circulation

Table 2 Data assimilated

Data	GLORYS	PSY3	PSY2	NCOM	HYCOM
Altimetry					
Jason-1	DM/NRT	NRT	NRT	NRT	NRT
ENVISAT	DM/NRT	NRT	NRT	NRT	NRT
GFO	DM/NRT	NRT	NRT	NRT	NRT
SST					
Satellite	NCEP RTG 0.5°	NCEP RTG 0.5°	NCEP RTG 0.5°	NCODA SST	NCODA SST
AOML drifters	No	No	No	Yes	Yes
Subsurface					
T, S					
ARGO	DM wQC	NRT wQC	NRT wQC	NRT wQC	NRT wQC
Moored buoys	PIRATA, wQC	PIRATA, wQC	PIRATA, wQC	PIRATA, wQC	PIRATA, wQC
other	XBTT, CTD, MBATHY, etc wQC				

NRT near real time, DM delayed mode, DM/NRT before Jan 23, 2008 DM and NRT thereafter, wQC with quality control, GFO Geosat Follow-on, NCODA SST see Gentemann et al. (2009)

Table 3 Data assimilation methods

Method	GLORYS	PSY3	PSY2	NCOM	HYCOM
IAU	Yes, 7-days	No	No	Yes, 1-day	Yes, 1-day
Scheme	Reduced order Kalman filter	Reduced order Kalman filter	Reduced order Kalman filter	NCODA MVOI	NCODA MVOI
Velocity initialisation	A	B	B	C	C

A statistical by-product of the analysis (progressive equatorial cutoff between 7° N/ 7° S), B physical balance operator, C NCODA MVOI, geostrophically balanced increments reduced to zero at 2° N/ 2° S

models that assimilate observational data. The exception is SURCOUF, which uses satellite altimeter data to obtain the geostrophic velocity and wind stress to obtain the empirically determined Ekman velocity. We will refer to all these velocity products as “models” although SURCOUF is more of an observational data product. While the reliability of model estimates over various integration time periods is an important test of model skill, our ranking of model skill was only applicable to the problem at hand; for example, the models with higher-frequency output have an advantage for this application that may not carry over to other applications that do not require high-frequency output (for a comparison of metrics, see, e.g. Metzger et al. 2010).

This paper is organized as follows: In Section 2, we delineate the study area and in Section 3, we describe the methodology used to estimate surface drifter trajectories. Then in Section 4, we present the trajectory estimate skill statistics of the six different models. In Section 5, we consider how to improve upon the estimates of the single OGCMs by combining them in an optimal way. We also describe the results of applying a spatial filter to the OGCM velocity fields, which both improved the estimates and allowed us to interpret the range of scales for which the models had useful skill. We conclude with a summary of the key results and their implications for further study in Section 6.

2 Study region

The comparison of various surface current estimates in the tropical Atlantic was first motivated by the need to perform drift computations in the context of the search of the wreck of the AF447 flight from Rio to Paris. The airplane disappeared on June 1st 2009 near 3° N and 31° W, and a large international effort was organized to try to find the wreckage. The contribution of oceanographers is described in (Ollitault 2010) and part of it in Drévilion et al. (2012). This region is very challenging

for ocean models because of tropical waves and especially for SURCOUF because of the breakdown in geostrophic balance at the equator.¹ Here we might expect the dynamics inherent in the OGCMs to provide complementary information to the observational data.

The choice of the size of the study region was a subjective compromise between choosing a larger area that included more surface drifters and therefore would provide better statistics and choosing a smaller area that was more homogeneous. We restricted calculations to drifters within the main study region: 10° S to 10° N, 60° W to 0° E, outlined in Fig. 1a. We studied the 18-month period from July 2007 to December 2008, the period when the models in Table 1 had a data assimilation scheme that remained unchanged.

In contrast to the midlatitudes, this region has mean flows that are comparable in strength to that of the time-varying flows. Figure 1a shows the kinetic energy (KE) of the 18-month mean flow (MKE) and the KE of anomalies relative to this mean (eddy kinetic energy, EKE) for the SURCOUF product. Interestingly, the mean currents reveal more sharply defined features associated with the narrow, zonally aligned current systems of the equatorial region. For example, note the MKE minimum from about 35° W to 0° at about 2 to 5° N, revealing the boundary between the eastward flowing north equatorial counter current (NECC) to the north and the westward flowing south equatorial current (SEC) to the south. We also represented in Fig. 1b the MKE and EKE fields for the ensemble multi-model product V5 described in Section 5. The V5 product is a combination of the surface velocity fields from the five OGCMs used in this study. We can notice that the MKE of V5 (Fig. 1b) is much smoother and less intense than in SURCOUF (Fig. 1a). The EKE field of

¹More properly, the meridional velocity becomes ageostrophic while the zonal geostrophic velocity becomes balanced with the vertical pressure gradient (Cushman-Roisin and Beckers 2010), which cannot be diagnosed from sea surface height measurements.

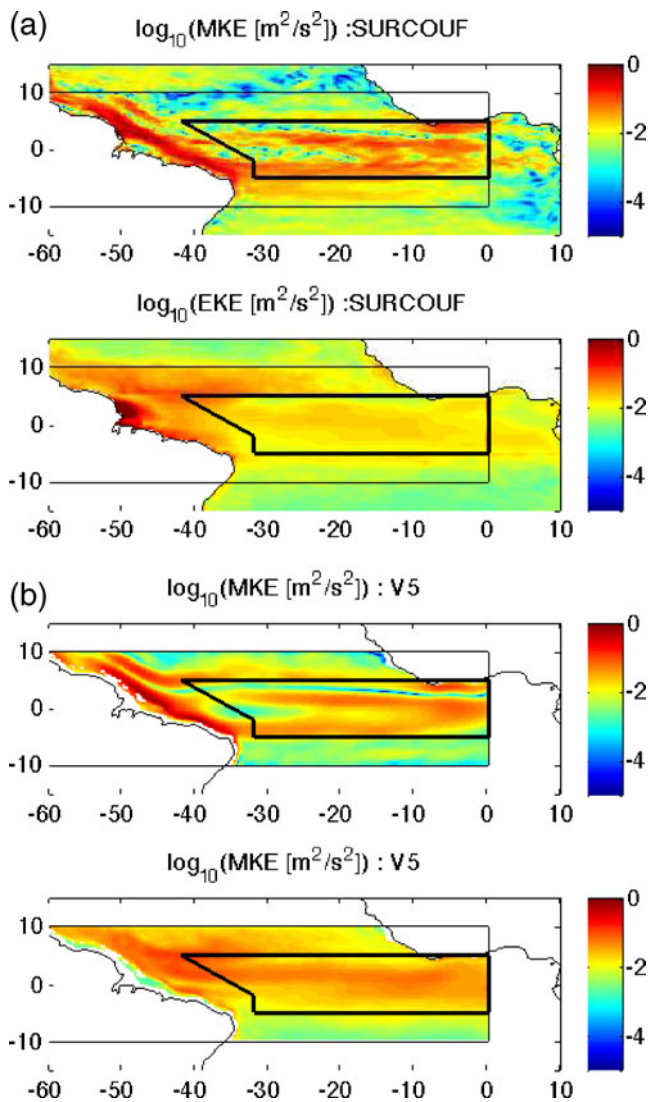


Fig. 1 **a** Upper panel kinetic energy of the 18-month mean flow from the SURCOUF product. Colour bar units are $\log_{10}(\text{m}^2/\text{s}^2)$. Lower panel corresponding kinetic energy of the current anomalies. Large rectangle outlined with thin straight lines indicates the main study region. Bold polygon outlines the equatorial subregion. **b** Like in panel (a) but for the five-model ensemble V5 product

SURCOUF and V5 looks also quite different. V5 has a stronger EKE along the equator. This may be related to the fact that OGCMs have daily outputs (NCOM outputs are even six-hourly snapshots) whereas SURCOUF surface currents comes from a linear interpolation between 7-day consecutive altimetry derived currents maps. We, however, can see that close to the Amazon river mouth, SURCOUF has a larger EKE than V5, which is most likely due to tide residuals in the SLA. One anticipates that it will be important for models to produce both accurate time variable and longer-term mean flows for accurate trajectory estimates.

As we will see later, there was a qualitative difference between the sharpness of the mean flow in the SURCOUF product and all of the OGCM mean flows.

In contrast to the sharply defined mean flows, the EKE was much more diffuse (cf. lower panel of Fig. 1a and b). This is due to the equatorial wave guide where linear waves (Rossby waves and equatorial Kelvin waves) (Chelton et al. 2007; Tulloch et al. 2009) travel along the equator. A relevant feature of the study region is the occurrence of tropical instability waves (TIWs) from late spring through to January (Weisberg and Weingartner 1988, Fig. 6). TIWs are surface-intensified structures of 600 to 1,200 km wavelength with phase speeds 20 to 50 cm/s and current speeds that often exceed 50 cm/s. The wave periods are typically 25 to 30 days (Weisberg et al. 1987; Cox 1980). TIWs are confined to the equatorial region, with EKE falling off very rapidly north of 4° N (see Jochum et al. 2004, Fig. 7). Despite the more linear dynamics of the tropics and wave periods of about a month, TIWs can evolve into highly nonlinear tropical instability vortices (TIVs), of about 500 km diameter with currents reaching over 1 m/s (Foltz et al. 2004). TIVs have been observed in both the Pacific (Kennan and Flament 2000) and the tropical Atlantic (Menkes et al. 2002; Foltz et al. 2004). OGCMs resolving the equatorial Rossby radius are generally able to simulate the observed structures (Dutrieux et al. 2008). The interannual variability of the TIWs is difficult to capture in a free-running (no data assimilation) numerical model forced with realistic forcing (von Schuckmann et al. 2008).

Another notable feature of the study region is the North Brazil Current (NBC) along the Brazilian coast. This current retroflects from May or June to December and feeds the North Equatorial Counter Current (e.g. Richardson and Reverdin 1987). The NBC retroflexion releases NBC rings that travel along the Brazilian coast towards the Lesser Antilles (Goni and Johns 2001; Barnier et al. 2001).

The large TIV interannual variability and the NBC rings make the central and western tropical Atlantic a region where currents can change quickly. Consider for example the historical time series at 3° N and 28° W from the SEQUAL mooring array deployed from 1983 to 1985, see Fig. 2. Around day 201 of 1984, the current jumped from weakly zonal to suddenly very strongly meridional within one day, see closeup in the lower panel of Fig. 2. These sudden jumps reveal a highly unstable current system characterized by strong intermittent currents reaching over 100 cm/s. For that particular event, it corresponds to a very intense westward propagating TIW reaching the SEQUAL surface mooring and changing abruptly the surface current intensity

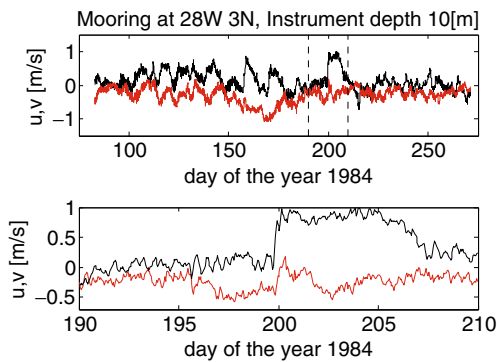


Fig. 2 Northward (*black*) and eastward (*red*) currents from the SEQUAL surface mooring near 28° W 3° N. Note the strong, chaotic, highly turbulent currents characteristic of this barotropically unstable region. The *vertical dashed lines* bracket a 20-day period with a particular strong meridional velocity pulse. *Lower panel* shows a close-up of these 20 days starting on day 190 of 1984 (mid-July)

(Weisberg and Weingartner 1988). This can be seen on a sequence of NOAA 1/4° SST maps (Reynolds et al. 2007, not shown).

Others have noted that trajectory estimate skill strongly depends on RMS current speed (Özgökmen et al. 2001; Barron et al. 2007). Thus, we anticipated that trajectory estimate skill for drifters in the strong current off the northwest corner of Brazil might be relatively low, while skill for drifters in regions with weaker currents (poleward of 7° N and 4° S) might be relatively high. Furthermore, SURCOUF velocities were computed using a different scheme near the equator (5° S to 5° N). For these reasons, we defined an equatorial analysis subregion (see Fig. 1a). Results from the main study region and the equatorial subregion will be contrasted in Section 4.2. Results in Sections 4.1, 4.3 and 5 were for the main study region only.

3 Forward trajectory methodology

We used the observed trajectories of satellite-tracked Surface Velocity Program (SVP) drifters of the Global Drifter Program (<http://www.aoml.noaa.gov/phod/dac/gdp.html>) from the AOML Drifter Data Assembly Center (www.aoml.noaa.gov/phod/dac/dacdata.html). The SVP drifters were drogued to follow the currents near 15 m depth, with the ratio of the drogue drag area to remaining drag area of at least 40. The wind-induced slippage of such drifters should be less than 1 cm/s in 10 m/s winds according to Niiler et al. (1995).

Since 2005, the drifters have been tracked with five or six satellites, with time between fixes usually between 1 and 2 h (Ellipot and Lumpkin 2008). We

used the quality-controlled drifters interpolated to six-hourly positions (Lumpkin and Pazos 2007).

For computational convenience, we divided the study period into three 6-month periods from July 1, 2007 through December 31, 2008. All the drifter trajectories for the first 6-month period are plotted in Fig. 3. For each drifter in the study region and for each forecast length $n \in \{1, 3, 7\}$ days, we simulated a set of trajectories using the following steps:

1. Start at its earliest location, check if the location is known n days later.
2. If so, estimate this later location using second-order Runge–Kutta (Heun’s method) integration of model 15 m velocity fields, bilinearly interpolated in space and time and using the model output time step. Trajectory error is defined as the distance (in kilometres) between the observed and estimated locations.
3. Check that each model simulated trajectory did not run aground. If this occurs, none of the model forecast is taken into account in order to have the same number of forecasts for each model.
4. Starting from the end time of the last forecast, repeat the above procedure (so forecasted trajectories do *not overlap* and can be treated as *independent*). If the start and end location of a drifter are not know, reject this time period and try 6 h later

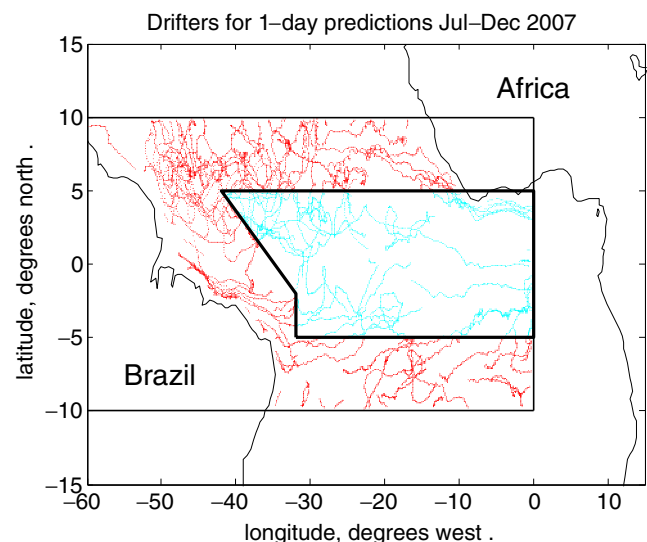


Fig. 3 Drifter tracks for the 6-month period of the study Jul 1, 2007 to Dec 31, 2007. *Red symbols* are the drifters outside the equatorial subregion. *Cyan symbols* are drifters within the equatorial subregion, which is also outlined by the *bold polygon* (roughly three times as many drifters were used for all the results of this study)

(i.e. no interpolation was done of the six-hourly data).

The skill of each model is then estimated by computing the median, RMS and 80th percentile of the trajectory forecast error over the ensemble of forecasts performed (see next section). We indicated the confidence of each statistic provided by a bootstrap method (Efron 1979). We also computed trajectories backward in time. The results for error statistics were the same as for the forward trajectories to within statistical uncertainty provided by the bootstrap method so we have only presented forward trajectories herein.

4 Single-model trajectory estimate skill results

Here, trajectory estimate skill statistics for 1-, 3- and 7-day trajectories are described for the six models shown in Table 1. Results are shown for the main study region (Section 4.1) and for the equatorial subregion (Section 4.2). In Section 4.3, we discuss the importance of the mean flow field.

4.1 Main study region

The skill of each model is summarized in the cumulative density plot of trajectory error in Fig. 4 and the corresponding statistics in Table 4. The 80th percentile of trajectory error can be interpreted as the radius of the circles about the estimated forward trajectory end point that contained 80% of the actual drifter locations. We could have shown PDFs, but we preferred to present the results with cumulative density functions (CDFs) because it is easier to read the median and 80th percentile on the figure. Furthermore, a CDF is inherently less noisy than the corresponding PDF. It is

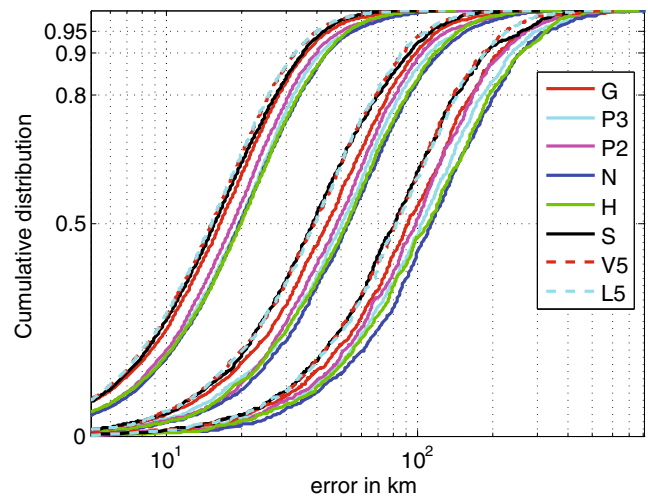


Fig. 4 Cumulative density functions of trajectory error for the main analysis region. The three clusters of lines from left to right are for 1-, 3- and 7-day estimates. Solid lines are for the six models, labeled by their first letter or two, e.g. HYCOM, shown in green, is labeled “H”, PSY2 is labeled “P2”. The comparison is made with exactly the same set of drifter trajectories, i.e. if an estimated trajectory ran aground or otherwise left the study region for one model, it was not counted for any of the models. Corresponding values tabulated in Table 4. The cyan dashed line, labeled L5, is the five-model ensemble of OGCMs (i.e. without SURCOUF) combined as in Eq. 1. The red dashed line, labeled V5, is the five-model ensemble of OGCMs combined as in Eq. 2

worth noting that the forecast error PDFs (not shown) are not Gaussian. They resemble the separation PDFs reviewed by LaCasce (2010) and are strongly asymmetrical. The PDF peak decreases and shifts towards larger separation distances with increasing trajectory time. We did not investigate further the properties of these PDFs as it is beyond the scope of this study.

The main result was that for 1-, 3- and 7-day trajectories, SURCOUF was at least as good and often

Table 4 Single model forward-trajectory error and 95% confidence limits for the main study region, Jul 1, 2007 to Dec 31, 2008

Qty	GLORYS	PSY3	PSY2	NCOM	HYCOM	SURCF
1-day	<i>N</i> = 7,360					
median	16 ± 0.3	20 ± 0.4	18 ± 0.4	20 ± 0.4	20 ± 0.4	16 ± 0.3
RMS	24 ± 0.5	28 ± 0.6	27 ± 0.6	29 ± 0.6	28 ± 0.5	23 ± 0.5
80%	28 ± 1	32 ± 1	31 ± 1	34 ± 1	34 ± 1	27 ± 1
3-day	<i>N</i> = 2,365					
median	44 ± 2	50 ± 2	48 ± 2	53 ± 2	52 ± 2	38 ± 1
RMS	66 ± 3	75 ± 3	72 ± 3	82 ± 3	77 ± 3	60 ± 2
80%	77 ± 3	86 ± 3	82 ± 3	93 ± 4	92 ± 4	70 ± 3
7-day	<i>N</i> = 933					
median	93 ± 6	104 ± 6	98 ± 6	114 ± 6	111 ± 8	80 ± 4
RMS	147 ± 10	160 ± 11	149 ± 9	175 ± 10	166 ± 10	128 ± 7
80%	164 ± 10	183 ± 12	167 ± 10	205 ± 12	196 ± 12	145 ± 10

80% means 80th percentile. Results shown graphically in Fig. 4
N the number of estimates

much better than the much more expensive OGCMs that all assimilated altimeter data. Of the OGCMs, Global Ocean Reanalysis and Simulations (GLORYS) made the best estimates, and NCOM made the worst estimates. Prototype Système 2 (PSY2) and Prototype Système 3 (PSY3) had similar skill though PSY2 was often slightly better. It seems that the quality of observations and the method used to assimilate them may be more important, since the GLORYS trajectories were the best among all OGCMs despite the fact that the GLORYS (and PSY3) grid also had the coarsest resolution. This highlights the importance of the data quality as GLORYS is a reanalysis using reprocessed and quality checked datasets whereas PSY2 and PSY3 operational outputs come from the real-time operation of the systems. The mode of data assimilation also has an impact as a smooth initialisation with incremental analysis update is used in GLORYS instead of sequential correction in (higher resolution) PSY2.

The forecast skill of a simple random walk model was also tested to see if the trajectory forecast in the models used would be similar to a diffusive process. To do this, we used the approach described in LaCasce (2008) (see their Eq. 23). The random walk model parameters are the local time average and root mean square of the velocity. In our case, we used the velocity fields from GLORYS. The results (not shown) indicate that the forecast skill of the random walk model is significantly worse than GLORYS. This shows that at the scales considered (1-, 3- and 7-day forecasts), the model currents are not a simple noise.

4.2 Equatorial subregion

Cumulative density plots of trajectory error for the equatorial subregion are shown in Fig. 5, with the

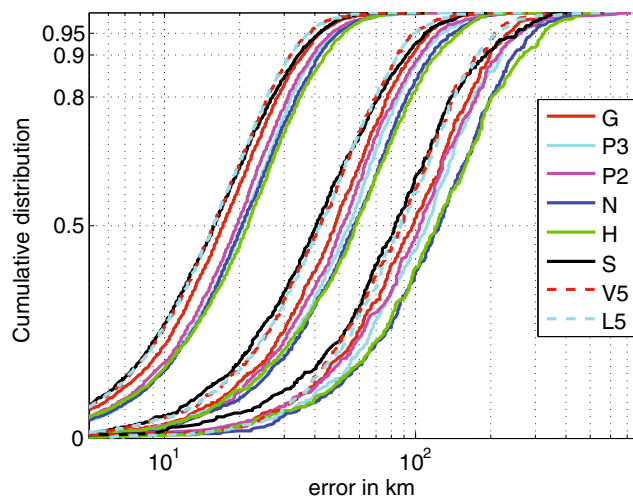


Fig. 5 As in Fig. 4 but for the equatorial subregion. Corresponding single-model values tabulated in Table 5

corresponding statistics summarized in Table 5. Results for this subregion are very similar to those for the main analysis region. In fact the trajectory errors are often slightly smaller for the equatorial subregion, though the differences are not significant at the 95% level. With only about 1/2 as many estimates (because of the smaller region), the statistical uncertainty was larger. In general, the model trajectory errors were similar. Note especially that SURCOUF consistently made the best estimates in the subregion as well, with the minor exception of the extreme tails of the distributions, cf. Fig. 5.

The similar, or perhaps slightly better, trajectory estimates in the equatorial subregion are both surprising and informative. Recall the elevated EKE associated with TIWs fell off quickly northward of 4° N and southward of 1° S (Jochum et al. 2004, Fig. 7), and TIVs form

Table 5 Like Table 4 but for the equatorial subregion outlined in Fig. 1a

Quantity	GLORYS	PSY3	PSY2	NCOM	HYCOM	SURCF
1-day	<i>N</i> = 3,864					
median	17 ± 0	21 ± 0	19 ± 0	20 ± 0	22 ± 1	16 ± 0
RMS	23 ± 1	27 ± 1	26 ± 1	27 ± 1	28 ± 1	22 ± 0
80%	28 ± 1	32 ± 1	31 ± 1	34 ± 1	35 ± 1	27 ± 1
3-day	<i>N</i> = 1,226					
median	48 ± 2	55 ± 3	52 ± 2	57 ± 3	58 ± 2	41 ± 2
RMS	64 ± 3	72 ± 3	70 ± 3	76 ± 3	79 ± 3	58 ± 2
80%	78 ± 3	86 ± 3	84 ± 4	94 ± 4	97 ± 5	72 ± 4
7-day	<i>N</i> = 477					
median	99 ± 9	110 ± 9	104 ± 7	121 ± 9	121 ± 9	85 ± 7
RMS	140 ± 13	151 ± 14	150 ± 13	163 ± 9	170 ± 10	124 ± 8
80%	167 ± 11	175 ± 10	176 ± 12	205 ± 15	209 ± 19	144 ± 12

The statistical uncertainty is greater because of the smaller numbers of estimates

along the high lateral shear zone between the NECC and SEC and are mostly found between the equator and about 5° N (Foltz et al. 2004, Fig. 5a). Thus, these challenging features are mostly *within* our equatorial subregion, and thus cannot be the sole reason limiting the performance of the OGCM trajectory estimates nor the sole reason for poor OGCM performance relative to the SURCOUF data product. This uniform performance of SURCOUF was surprising since geostrophic balance “breaks down” in the equatorial region, and close to the equator, only the zonal velocity component of the velocity is deduced from SLA.

4.3 18-month mean flow

Given the relatively strong mean flows in the tropical Atlantic, a natural question is whether the 18-month mean flow of SURCOUF was perhaps superior to that of the OGCMs. In Figs. 6 and 7, we plot the mean zonal and meridional velocity fields, respectively, for several of the models. All three Mercator-Océan OGCM (i.e. GLORYS, PSY3, PSY2) mean fields were so similar that they were difficult to distinguish visually and thus only GLORYS is presented. While there are slight differences between GLORYS and Hybrid Coordinate Ocean Model (HYCOM) in both fields, the most unique field is the zonal velocity of SURCOUF, with sharply defined structures such as the SEC. To test whether both the mean and the eddy fields of SURCOUF had more skill than the corresponding OGCM fields, we performed in the main region several experiments in which we replaced the SURCOUF mean

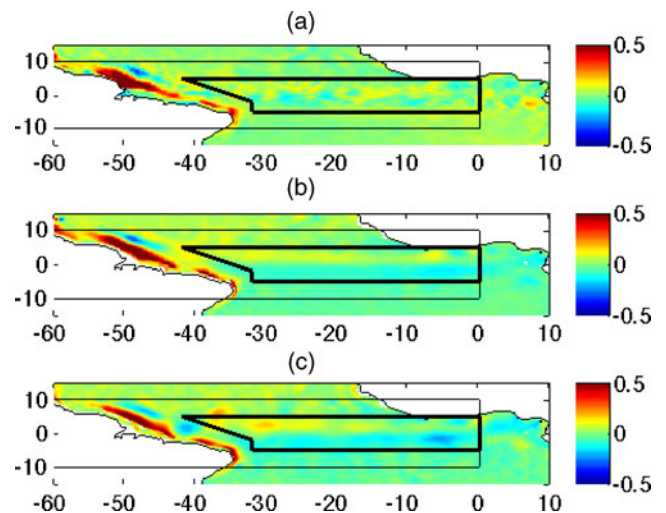


Fig. 7 As in Fig. 6 but for the meridional velocity

fields with those from other models. In all cases, the trajectory errors increased although not always enough to be statistically significant at the 95% level. This was true even for the V5 ensemble (defined in Section 5). This confirmed that the fine structures in Fig. 6a were an improvement over the more diffuse mean zonal velocities of the OGCMs.

One can also ask whether the mean field of SURCOUF was the most important factor? That is, perhaps the eddy field of SURCOUF was actually inferior to the OGCMs, but the deficiency was compensated for by the superior mean field? We confirmed that this was *not the case*. We replaced the GLORYS mean field with that of SURCOUF and found that, while this improved the trajectory estimates over that of GLORYS alone, the estimates were still inferior to SURCOUF alone. That is, the eddies of SURCOUF were also superior to the eddies of GLORYS. However, as we will see in the next section, the ensemble average of all the OGCMs, V5, made better trajectory estimates than SURCOUF. This occurred despite the fact that its mean field was inferior to that of SURCOUF. Thus, the V5 ensemble seems to have superior eddies than SURCOUF, although this could not be explicitly verified.

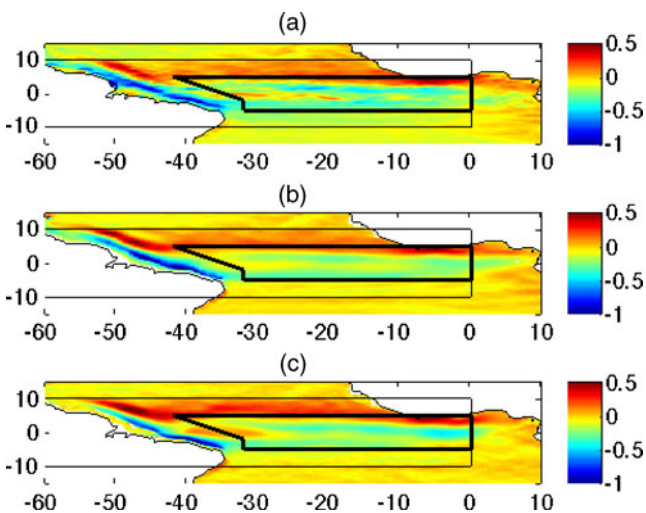


Fig. 6 Eighteen-month mean zonal velocity field for **a** SURCOUF, **b** GLORYS and **c** HYCOM

5 Improving model trajectory estimates

We might expect that somehow combining models might improve the trajectory estimates. The benefits from ensemble forecasts on predictability has been noticed first by Leith (1974), more than three decades ago. The idea behind ensemble forecasting is that an ensemble of analyses or forecasts will better sample the true

state than a single member (deterministic forecast). By averaging the ensemble members, one gets an improved true-state estimation than with a single member. A comprehensive description of the ensemble forecasting concept is given by Murphy (1988). More recently, the “super ensemble” approach of optimally combining several different model estimates has been successfully used in ocean forecasting (Rixen and Ferreira-Coelho 2007; Rixen et al. 2008, 2009). However, for the application explored herein, the best method to combine models is not a priori obvious. On the one hand, one could first use each model to make an estimate and then combine those estimates. The advantage with such a method is that each model is internally dynamically consistent. On the other hand, one could combine the model velocity fields and make estimates with these compromise velocity fields. The apparent advantage of such a method is that trajectory errors accumulate during the trajectory integration so it might be best to reduce errors in the velocity fields *before* using them for integration. Furthermore, the compromise velocity fields should be smoother, reducing the noise we expect to dominate at small scales. Below we describe the results from employing these two strategies. We also address the possibility of improving the single-model estimates by applying a low-pass spatial filter to the velocity fields. This analysis allowed us to identify the range of length scales with useful skill for both the individual OGCMs and the five-model compromise.

5.1 Four- vs. five-model ensembles

We computed compromise forecasts from an ensemble of four or five models. Consider the “model

compromise forecast”, as the weighted average of the estimated locations:

$$\begin{aligned}x_{\text{ens}} &= \sum_{m=1}^M w_m x_m \\y_{\text{ens}} &= \sum_{m=1}^M w_m y_m\end{aligned}\quad (1)$$

where x_m and y_m are the estimated longitude and latitude of the forward trajectory integrations for model m . For weights we used, $w_m = V_m^{-1} / \sum_{n=1}^M V_n^{-1}$, where V_m was the mean square error for model m for the corresponding forecast length. For the ensemble of all five OGCM models, the sum is over $m \in \{1, 2, \dots, 5 = M\}$.

Statistics for the trajectory errors corresponding to the five-model ensemble are presented in the seventh column of Table 6, labeled “ALL”. We also considered removing one model from the ensemble. The results for these four-model ensembles are also presented in Table 6 in columns 2 through 6. The column label indicates the model *withheld* from the ensemble. Note that none of the columns has trajectory error consistently lower than the seventh column. This indicates that none of the models consistently degraded the five-model ensemble estimate. All models “contributed” in the sense that including them in the five-model ensemble made for a better estimate or at least not a worse estimate.

We expect the improvement from the multi-model ensemble to arise from the cancellation of random model trajectory errors. Ideally all the models would provide independent estimates, so their errors would be unrelated and tend on average to cancel. The cumulative density function for the five-model OGCM ensemble, composed of GLORYS, PSY3, PSY2, NCOM and HYCOM combined as in Eq. 1, was plotted in Fig. 4. This compromise estimate composed of only OGCM

Table 6 OGCM model ensemble forward trajectory error and 95% confidence limits for the main study region for time period July 1, 2007 to Dec 31, 2008

Qntity	GLORYS	PSY3	PSY2	NCOM	HYCOM	ALL
1-day	$N = 7,360$					
median	16 ± 0.3	15 ± 0.3				
RMS	23 ± 0.4	22 ± 0.4	22 ± 0.4	21 ± 0.4	22 ± 0.4	21 ± 0.4
80%	27 ± 0.5	26 ± 0.5	26 ± 0.5	26 ± 0.4	26 ± 0.5	26 ± 0.4
3-day	$N = 2,365$					
median	41 ± 1	39 ± 2	40 ± 1	39 ± 1	40 ± 1	39 ± 1
RMS	60 ± 2	58 ± 2	58 ± 2	57 ± 2	59 ± 2	57 ± 2
80%	71 ± 3	68 ± 2	69 ± 2	68 ± 2	69 ± 2	68 ± 2
7-day	$N = 933$					
median	88 ± 4	84 ± 5	84 ± 4	84 ± 3	85 ± 5	82 ± 5
RMS	127 ± 7	125 ± 8	124 ± 6	122 ± 7	126 ± 7	122 ± 7
80%	149 ± 8	145 ± 9	149 ± 7	142 ± 9	149 ± 8	143 ± 7

The seventh column “ALL” is for the weighted average of all five OGCM models. The remaining columns, second through sixth, are for the average of four models. So the second column is for all *but* the GLORYS model. The higher trajectory error for the second column indicates that *removing* GLORYS from the ensemble *worsens* the ensemble estimate. None of the models were found to consistently worsen the estimates

results was clearly as good as or sometimes better than the data product SURCOUF and all the individual model estimates. This result further supports the idea of partial cancellation between model trajectory errors.

5.2 Combining model velocity fields

Another strategy for combining model estimates is to average the velocity fields from an ensemble of models and make a single integration with the ensemble velocity field. Consider the “model compromise velocity”, as the weighted average of the velocity from the individual models:

$$\begin{aligned} u_{\text{ens}} &= \sum_{m=1}^M w_m u_m \\ v_{\text{ens}} &= \sum_{m=1}^M w_m v_m \end{aligned} \tag{2}$$

where u_m and v_m are the zonal and meridional velocities for the 15-m currents for model m , linearly interpolated onto a common grid. For weights we used, $w_m = V_m^{-1} / \sum_{n=1}^M V_n^{-1}$, where V_m was the mean square error for model m for the 7-day trajectory forecasts. For the common grid, we used that of the GLORYS model. Note that this effectively coarsened the spatial resolution of all models except PSY3 and coarsened the temporal resolution of NCOM. We expect the spatial coarsening had negligible effect based upon the results of our smoothing experiments reported in the next subsection. We confirmed that the temporal smoothing had negligible effect by repeating the experiment using the NCOM temporal resolution (six hourly) and found agreement well within statistical uncertainty. Hereinafter we will refer to these fields as “V5”.

The empirical cumulative density function of trajectory error corresponding to V5 ensemble was plotted in Fig. 4 with a dashed red line. Interestingly, both strategies for combining the model estimates gave similar results (both red and cyan dashed lines are similar). And regardless of the strategy to combine the model estimates, the five-model OGCM ensembles (super ensembles) both worked better than all the individual OGCMs and had similar skill and sometimes better skill than the data product SURCOUF.

5.3 Smoothing velocity fields

One might speculate that combining the velocity fields as in Eq. 2 led to smoother velocity fields. Pessimistically one might conjecture that the improved estimates occurred only because of the smoothing (Wunsch 2010, personal communication), a position we will call the null hypothesis. More generally, it seems plausible that the errors in the OGCM velocity fields were a strong

function of spatial scale with larger errors at smaller scales. This raises the question as to what length scales have useful skill and what scales are too small to be captured by the OGCMs. To address this question, we have applied a low-pass filter to the OGCM velocity fields prior to Runge–Kutta trajectory integration. The low-pass filter was accomplished by convolving the original OGCM velocity fields at each time step and each grid point (x_0, y_0) with a Gaussian filter,

$$G(x, y; x_0, y_0) = A \exp\{-[(x - x_0)^2 + (y - y_0)^2] / (2R^2)\},$$

with Gaussian radius R , over a square region centred at (x_0, y_0) and of width $2R$, with A chosen so that the sum of weights was unity. For each OGCM, many experiments were performed with R ranging from a few tens of kilometres to hundreds of kilometres, each experiment using only one application of a given filter to the original velocity fields.

There appeared to be an optimal smoothing radius in the range $100 \lesssim R \lesssim 200$ km that produced the best estimates. This is shown with the 80th percentile of the 7-day trajectory error plotted in Fig. 8 versus smoothing radius R . The corresponding plot for the RMS error is shown in Fig. 9. The y -intercept, corresponding to $R = 0$, corresponds to the result with no smoothing at all, for which values can also be read from the final two rows of Table 4, though agreement is not exact since

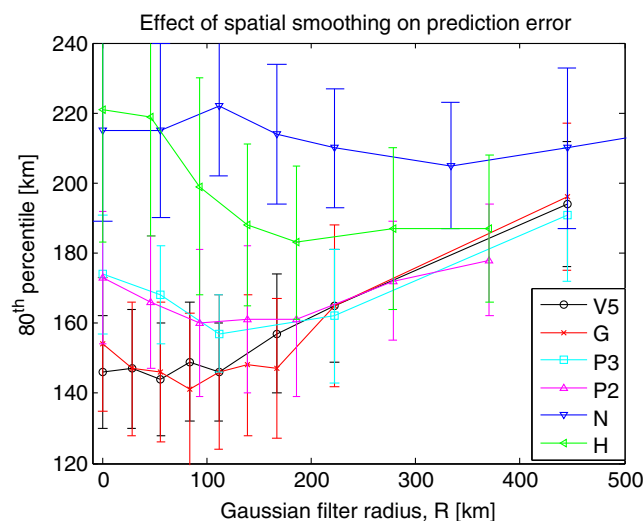


Fig. 8 Eightieth percentile of 7-day trajectory error (kilometres) vs. smoothing radius (kilometres) for each OGCM. Analysis performed in main study region. *Line* labelling described in Fig. 4 caption. *Error bars* represent the formal error 95% confidence limits. Discrepancies between the Y -intercept values and the final row of Table 4 arise because different trajectories were used. Here near coastal trajectories were eliminated when the velocity fields were smoothed

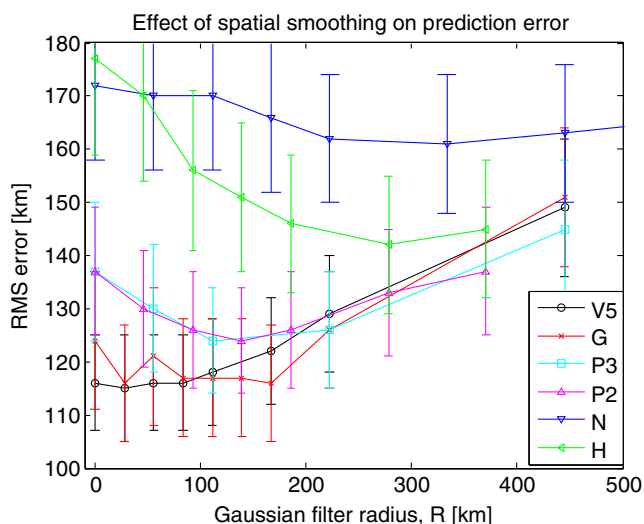


Fig. 9 As in Fig. 8 but for the RMS error. Discrepancies between the Y-intercept values and the penultimate row of Table 4 arise because different trajectories were used. Here near coastal trajectories were eliminated when the velocity fields were smoothed

trajectories near the coasts were necessarily omitted from Figs. 8 and 9, due to the smoothing. In fact the discrepancies underline the importance of always making comparisons with the same set of drifter trajectories because of the long tails in the PDFs. Error bars represent the 95% confidence interval obtained with bootstrapping with 1,000 subsamples. Because of the large statistical uncertainty, it is necessary to consult both Figs. 8 and 9 to confirm the trends. The local minimum in trajectory error was qualitatively reproduced in both statistics, with the exception of the 80th percentile for PSY2.

The interesting exception to the optimal smoothing radius was the model constructed from all five OGCMs as per Eq. 2, labeled V5 in Figs. 8 and 9, which showed little or no improvement for small-scale smoothing, and errors worsened noticeably for $R \gtrsim 75$ km. The errors continued to grow monotonically and rapidly through to the largest filter radius considered, $R \approx 450$ km. That is, the optimal smoothing radius was indistinguishable from zero (no smoothing) and was at most about 75 km. Unfortunately it was difficult to be more precise because the 95% confidence limits were fairly large. Accounting for the statistical uncertainty, one can say the V5 results in Figs. 8 and 9 show with 95% confidence that the trajectories with about 150 km or larger smoothing were worse than those with no smoothing. This implies that there is at least some skill in length scales less than 150 km. However, the smoothness of the curves and the consistency of the 80th percentile of the 7-day trajectory error and RMS

error suggests these are conservative confidence limits. The smaller optimal smoothing radius, between 0 and 75 km, for V5 compared to 100 to 200 km for any of the individual OGCMs suggests that V5 had skill at smaller scales. Our interpretation is that buried in the noise at small scales, the individual OGCMs had some skill down to about 75 km or smaller. Combining the velocity fields to produce the compromise model V5 allowed us to reduce the small-scale noise and exploit that skill. This result is consistent with the results obtained by Murphy (1988). Based on both numerical results and simple theoretical estimates, Murphy (1988) showed that an “ensemble-mean forecast is more skilful than an individual forecast”. Spatial smoothing should also improve the skill of both an individual and an ensemble-mean forecast, but the ensemble mean forecast remains superior. The explanation is that an ensemble-mean forecast provides a better estimate of the true ocean circulation than a single one. However, because of the statistical uncertainty, these conclusions are not definitive.

From a practical point of view, one would like to choose the best model to make forecasts. Comparing the 80th percentile and RMS trajectory errors in Figs. 8 and 9, it appears that V5 with no smoothing and GLORYS are the two best and the differences

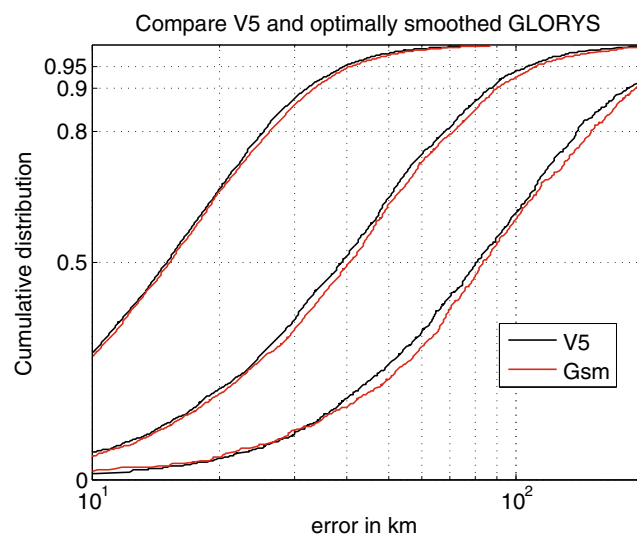


Fig. 10 CDF of trajectory error as in Fig. 4 but comparing the optimally smoothed GLORYS model, red line (smoothed with Gaussian radius of about 167 km) and V5 model, black line (not smoothed). The comparison is made with exactly the same set of drifter trajectories. Because the compromise V5 model is consistently better than the best of the OGCMs for 1-, 3- and 7-day trajectory estimates, we have grounds to reject the null hypothesis that forming the compromise model improves estimates only because it has smoother velocity fields

between them are not statistically significant at the 95% confidence. The 80th percentile and RMS represent only two statistics derived from the full distribution. It is informative to compare the full distribution by comparing the CDFs. Figure 10 shows the CDF of trajectory error for GLORYS optimally smoothed ($R = 160$ km) and V5 with no smoothing. V5 is consistently better but because the improvement is only slight, it is not statistically significant at the 95% level. This provides evidence against the null hypothesis that the ensemble was better only because it was smoother. Unfortunately with the limited data available, we cannot reject the null hypothesis with 95% confidence. One factor to bear in mind is that the weights used in the optimal model combination done using Eqs. 1 and 2 could be a function of the filter radius used in the smoothing, yet the weights for V5 were chosen from the RMS error with no smoothing. The change of the individual model skill with the spatial smoothing rather supports this hypothesis.

6 Summary and discussion

Ocean state estimation with data assimilation in OGCMs with sufficient resolution to produce an energetic mesoscale eddy field that dominates the advection of surface drifters is a very young science. Adding quality to the observational data is clearly a great challenge. Evidence of the great challenge was presented herein, where the data product, SURCOUF, revealed more skill than the five individual data-assimilative OGCMs in estimating the trajectories of surface drifters. The OGCMs all assimilated the altimeter data upon which the SURCOUF data product was based. Furthermore, our results were for the equatorial Atlantic where SURCOUF faced the additional challenge that the geostrophic balance breaks down within about 5° of the equator. In this version of SURCOUF, the calibration of the velocity anomalies was completely independent of the AOML drifters from our study period. However, recall the mean currents in SURCOUF were dependent on the AOML drifters used herein, but the dependence was barely significant at the 95% level, see discussion in the “Appendix”. Another important fact is that SURCOUF, as a data product, is inherently limited to estimates of past events, while in principle the OGCMs run in an operational configuration can make predictions of the future, although we did not assess future predictions herein.

We found median 1-day trajectory errors between about 15 and 20 km. This is consistent with results found with the US Navy EAS16 model in the

East China Sea (Huntley et al. 2011). Barron et al. (2007) found that trajectory estimation accuracy was regionally dependent. Although their NCOM Equatorial Atlantic results (16 to 18 km) fall within the range we found for all models, they found better results with NCOM than we did, presumably because their region extended to $\pm 15^\circ$ and thus included more quiescent regions. Trajectory error of course increased with time and by 7 days we found median errors between about 80 and 115 km, also broadly consistent with Barron et al. (2007).

In practice, controlled experiments with eddying OGCMs with data assimilation are extremely costly in terms of both researcher time and computational resources and need to be well justified. Much can be learned from the inter-comparison of existing runs, and the results described herein motivate further study. Our results of accuracy of estimated drifter trajectories begs the question why SURCOUF had more skill than the OGCMs especially since all the OGCMs assimilate the altimeter data used to construct SURCOUF. While the two NRL OGCMs both used Navy Operational Global Atmospheric Prediction System (NOGAPS) winds, the three Mercator-Océan OGCMs all used ECMWF winds, as did SURCOUF. This raises questions as to whether the temporal resolution of the winds is an important factor since SURCOUF used the six-hourly Interim winds from ECMWF while the Mercator-Océan OGCMs were forced with daily averaged operational ECMWF winds.

We speculate that some benefit could be obtained by forcing the OGCMs with the six-hourly winds rather than daily averages. Indeed, inertial ocean motions are forced by moving storms when the wind vector rotates at a frequency close to the local inertial frequency f (e.g. Price 1981, 1983). The inertial period $2\pi/f$ is about 2.9 days near 10° N, and therefore, the rotation of the wind stress is poorly described with a daily forcing. Finally, we speculate that using a six-hourly solar forcing may have stronger consequences than using a six-hourly wind forcing (as compared to daily forcings), as found by B. Barnier (personal communication) in the Mediterranean Sea.

None of the models included tidal forcing, which in the deep ocean leads to errors similar to that due to slippage in strong winds, about 1 cm/s. However, this is unlikely to be a dominant factor, contributing only about a kilometre per day to the error.

It is instructive and perhaps surprising that one of the lowest resolution OGCMs, GLORYS, had the best skill of all the OGCMs. The fact that the higher-resolution PSY2 was marginally better than its lower-resolution counterpart PSY3 suggests that resolution is

by no means a hinderance and perhaps improves the estimates marginally. Recall from Tables 2 and 3 that GLORYS had two clear advantages over its counterparts at Mercator-Océan: The Jason-1 and ENVISAT altimeter data and ARGO and other T&S data were used in delayed mode instead of near real time. Delayed mode allows for quality control with removal of outliers and other suspect data. Furthermore, GLO- RYS integrated the incremental analysis update (IAU) scheme in the data assimilation method (Bloom et al. 1996; Benkiran and Greiner 2008), which is believed to be an improvement. The results described herein strongly motivate controlled experiments to decisively determine the relative importance of data quality and data assimilation scheme in producing the enhanced skill of GLORYS over PSY3 and PSY2.

Evidence that the OGCMs can add value to the data was obtained from the result that compromise estimates employing all the OGCMs had skill as good or better than SURCOUF. Two strategies for combining the OGCM results to produce compromise estimates were explored. We tried averaging the latitude and longitude of the estimated trajectory from each model, weighted by its mean squared error. And we tried averaging the OGCM velocity fields to produce a single, compromise velocity field that was used to make trajectory estimates. The results were very similar for both ensemble methods and always better than the best single model, GLORYS; compare the “ALL” column of Table 6 and “GLORYS” column of Table 4. The ensemble trajectory estimates were almost always better than the SURCOUF estimates, though not always statistically significantly so; compare the “ALL” column of Table 6 and “SURCF” column of Table 4. The fact that a multi-model ensemble better fits the observational signal and improves the skill is consistent with the results from Murphy (1988) where the superiority of an ensemble-mean forecast over an individual forecast was shown both with numerical ensemble forecasts and simple theoretical considerations. The result from the present study points to interesting prospects for the users of operational oceanography forecasts.

We also noted that most OGCMs had an “optimal low-pass filter radius”, i.e. removing scales smaller than roughly 150 km or so improved the estimates. The interpretation is that the OGCM’s surface velocity fields contain errors that increase in importance with smaller scales. Below about 150 km, the errors are more important than the signal (importance assessed by impact on Lagrangian particle trajectories). These errors can be attributed to various sources. Models suffer from shortcomings like their lack of resolution, errors in the

forcing fields or bulk parameterisations used which all contribute to the forecast errors. And at the scales considered (spatial scales less than the Rossby radius and time scales less than 7 days), the nonlinearities of the advection terms in the momentum equations are more important than at larger scales and are able to strongly amplify small initial errors. Furthermore, all numerical models include data assimilation where the model state is corrected sequentially. The analysis may introduce some shocks when the increments are applied, i.e. the thermodynamics may be slightly unbalanced, especially at the equator where geostrophic balance does not hold. This may introduce some noise in the surface currents, especially when incremental analysis update is not used (Ourmieres et al. 2006). Lastly, the observational network is certainly not sufficient to correctly constrain the full dynamics. All these factors contribute to small-scale errors. By filtering the small scales, one removes those errors and one obtains an ocean state estimation closer to the true ocean. As a consequence, the trajectory forecast skill is improved. This result is also in agreement with Murphy (1988) who showed that spatial filtering improves both ensemble-mean and individual forecasts. Our result is also partially consistent with the results of Huntley et al. (2011) who found that coarsening the US Navy EAS16 model velocity fields in space (or in time) by up to a factor of 8 via subsampling did not degrade the trajectory estimates. However, buried in those errors, there appeared to be some useful signal. This was suggested by the fact that the optimal filter for the compromise velocity field that averaged the five models as in Eq. 2 was between 0 and about 75 km and thus smaller than the 100- to 200-km optimal filter of the individual OGCMs. The ensemble velocity fields may have had skill on smaller scales. Furthermore, ensemble velocity fields had greater skill than even the best single model optimally smoothed, see the CDF of trajectory error in Fig. 10. But because the improvement is only slight, it is not statistically significant at the 95% level.

Acknowledgements Eric Greiner suggested to combine model ensemble velocity fields (personal communication, 2010). The null hypothesis that the model ensemble velocity fields have more skill only because they were smoother came from Carl Wunsch (personal communication, 2010). The presentation of the manuscript benefitted substantially from two anonymous reviews. RBS thanks the National Oceanography Centre, Southampton (NOCS) for hosting an extended visit. RBS was supported by National Science Foundation grants OCE-0526412 and OCE-0851457 and NASA subcontract through Boston University and NOCS. This is UTIG contribution #2481.

Appendix: Models

Description of PSY2 model runs

Mercator-Océan PSY2 is an operational ocean analysis and forecasting system based on the NATL12 ocean configuration and a reduced order Kalman filter data assimilation scheme. The NATL12 ocean model configuration is a regional implementation of the ocean/sea-ice NEMO numerical framework (Madec 2008) carried out by Mercator-Océan and the European DRAKKAR collaboration (DRAKKAR Group 2007). The configuration is similar in many points to the one used by Barnier et al. (2006) except that the resolution is $1/12^\circ$ (Mercator grid) and that the geographical domain is limited to the North Atlantic (20° S– 70° N) and the Mediterranean Sea. The model has 50 layers in the vertical (Z coordinate), with a layer thickness of 1 m near the surface, increasing with depth (10 m at 50 m depth) up to 450 m at 5,500 m depth. It uses a partial step representation of the bottom topography and a momentum advection scheme that both yielded significant improvements (Penduff et al. 2007). Parameterisations include a Laplacian mixing of temperature and salinity along isopycnals, a horizontal biharmonic viscosity and a turbulence closure scheme (TKE) for vertical mixing. The turbulent surface fluxes are computed using the CLIO bulk formulation (Goosse et al. 2001) forced by ECMWF operational analyses (1-day averages). The surface wind stress is the one provided by ECMWF analyses (i.e. it is not computed using the CLIO formulation). The ocean model includes the river runoff climatology of Dai and Trenberth (2002).

The data assimilation scheme is based on the singular evolutive extended Kalman filter formulation proposed by Pham et al. (1998). This approach has been used for several years at Mercator-Océan and was implemented in different ocean (re)analysis systems like PSY2, PSY3 (http://bulletin.mercator-ocean.fr/html/welcome_en.jsp) or GLORYS (see below). Details about the implementation of the data assimilation scheme are described by Tranchant et al. (2008). A key aspect of the method is the use of a large number of model anomalies (a few hundred) to model explicitly the background model error covariance. In PSY2, the control vector consists of the barotropic height and the temperature and salinity fields. In order to produce a balanced, analysed ocean state the velocity is deduced from the barotropic sea surface height and mass field increments using appropriate physical balance operators. Among them, a linear equation of baroclinic motion is used to build the baroclinic velocity increments near the

equator (see Benkiran and Greiner (2008)). The length of the assimilation cycle is 7 days, and the increment is applied directly to the model state at the analysis time. The assimilated data is sea level anomaly (in conjunction with the mean dynamic topography of Rio and Hernandez (2004)), SST and in situ profiles (see Table 2).

Description of PSY3 model runs

Mercator-Océan PSY3 is very similar to PSY2 (see above) except for the following principal differences. The spatial resolution was coarser ($1/4^\circ$ Mercator grid). Furthermore, the error covariance statistics were different since they were computed from a reference experiment with no data assimilation for each model configuration. Finally, the SST observation operator was slightly different, with less smoothing of the model equivalent for PSY3, and slightly different weights applied.

Description of the GLORYS model runs

GLORYS is a project with objective to produce a series of realistic (i.e. close to the existing observations and consistent with the physical ocean) eddy resolving global ocean reanalyses. The version 1 of stream 1 (called GLORYS1V1) covering the Argo years (2002–2008) is used in this study. The ocean reanalysis system used in GLORYS is similar in many points to PSY2. However, some important differences exist that we review in the following. The OGCM used in GLORYS1V1 is also based on the ocean/sea-ice NEMO numerical framework (Madec 2008). The main differences with PSY2 are: (a) the configuration is global (-77° S to the North Pole) and (b) the horizontal resolution is coarser ($1/4^\circ$ Mercator grid). GLORYS1V1 shares the same vertical grid as PSY2. The physical parameterisations used are basically the same, except that GLORYS has an additional harmonic diffusion operator in the tropical band (5.5° N/ 5.5° S) to improve the tropical instability wave physics at $1/4^\circ$ horizontal resolution. The data assimilation scheme is close to PSY2, except that the control vector includes two more variables: the zonal and meridional velocity components. This allows producing a velocity increment consistent with the analysed mass field and model physics. Because there is no simple relationship between the mass field and the circulation near the equator (e.g. Benkiran and Greiner 2008), the analysed velocity near the equator is only partially applied. The velocity increments are set to zero at the equator and increase smoothly with

latitude to become maximal at 7°. The last important difference with PSY2 is the use of an IAU initialisation procedure (Bloom et al. 1996) to apply the increment to produce a time continuous ocean analysis.

Description of NCOM model runs

The 2007–2008 NCOM results are from the global ocean forecast system (GOFS) version 2.6 running operationally at the Naval Oceanographic Office. Global NCOM (Barron et al. 2006) uses a rotated bipolar curvilinear grid with spacing about 20 km at the equator, 14 km (1/8°) at midlatitudes and 5 km in the Arctic. It employs an implicit-free surface and hybrid vertical grid with 19 terrain-following sigma levels above 21 fixed-level z coordinates below 141 m, chosen to be near the depth of a typical shelf break. The layers are logarithmically stretched below a 1-m-thick uppermost layer. In GOFS 2.6, data assimilation (Barron et al. 2007) relaxes to a background of Modular Ocean Data Assimilation System (Fox et al. 2002) synthetic profiles of temperature and salinity derived based on remote observations of sea surface height and sea surface temperature and modified by in situ observations through the Navy Coupled Ocean Data Assimilation System (NCODA; (Cummins 2005)). GOFS obtains wind stress and surface heat flux forcing from the NOGAPS (Rosmond et al. 2002). River inflow is derived from a monthly climatology for 981 of the world's largest rivers (Barron and Smedstad 2002). Tides are not included in the present global model and are optionally added in a separate step when nesting a higher-resolution regional model. Simulated drifter evaluations with earlier versions of global NCOM were performed by Barron et al. (2007) and van Sebille et al. (2009).

Description of HYCOM model runs

HYCOM is widely used by the ocean community (<http://www.hycom.org>) and is the backbone of the global eddy-resolving (1/12° horizontal resolution) real-time nowcast/forecast system at the Naval Oceanographic Office. The model has nominal 1/12° Mercator grid horizontal resolution (6.5-km grid at midlatitudes with a bipolar patch north of 47° N, i.e., 3.5-km grid spacing at the North Pole) and 32 hybrid layers in the vertical (pressure coordinates are used in the mixed layer, isopycnal coordinates are used in the ocean interior and terrain-following coordinates are used in shallow areas) (Bleck 2002; Chassignet et al. 2003, 2006, 2009).

The simulation used for the analysis here was restarted from a spun-up state of a non-assimilative

global 1/12° HYCOM simulation with climatological forcing. The assimilative hindcast began in May 2007 and integrated through the analysis period while being forced by the three-hourly NOGAPS (http://www.nrlmry.navy.mil/nogaps_his.htm) wind stress, wind speed, heat flux (using bulk formula) and precipitation. Runoff from 986 rivers was included as virtual salinity flux with no mass exchange. The 1/12° assimilative global HYCOM system has been validated by Metzger et al. (2008, 2010).

The data assimilation in HYCOM is performed using the NCODA system. NCODA is a multivariate optimal interpolation scheme that assimilates surface observations from satellites, including altimeter and multi-channel sea surface temperature data, sea ice concentration and also profile data such as XBTs, CTDs and profiling floats (Cummins 2005).

Description of SURCOUF

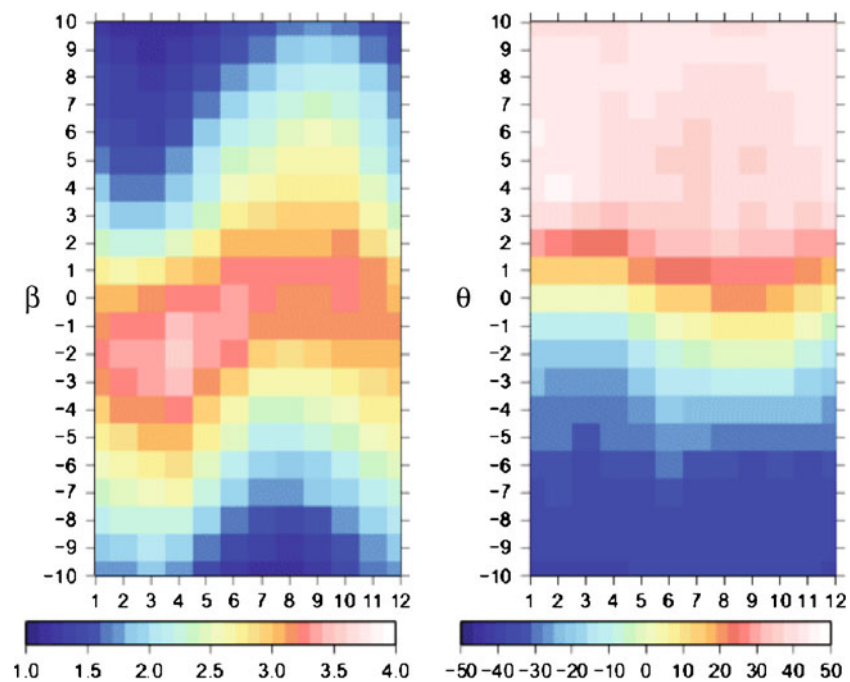
The SURCOUF currents were computed globally at a six-hourly temporal resolution using the following methodology that combines estimates of geostrophic current and the Ekman component of the ageostrophic current. Daily geostrophic currents were obtained from the gradient of the global multi-mission altimetric maps distributed by AVISO. The mean dynamic topography (MDT) used to reference the sea level anomalies was the recent solution computed by Rio et al. (2011) using the following three-step method (Rio and Hernandez 2004). First, a large-scale mean dynamic topography was obtained from the CLS01 altimetric mean sea surface (Rio and Hernandez 2004) and a geoid model computed at Groupe de Recherches de Géodésie Spatiale, Toulouse from 4.5 years of GRACE data. Then, in situ measurements (drifting buoy velocities from 1993 to 2008, CTD casts and ARGO profiles from 1993 to 2007) were combined with altimetric anomalies to compute synthetic estimates of the MDT and the corresponding mean currents. The synthetic estimates were finally used to improve the large-scale solution through a multivariate objective analysis.

Six-hourly ERA INTERIM wind stress fields (Berrisford et al. 2009) were used to compute maps of Ekman currents \vec{u}_{ek} through the use of a simple statistical model:

$$\vec{u}_{ek} = \beta \exp(i\theta)\vec{\tau},$$

where β and θ have been obtained analysing 15-m drogued drifting buoy velocities that were collected in the framework of the international Global Drifter Program, quality-controlled and distributed by the AOML center. To estimate \vec{u}_{ek} , absolute altimetric velocities

Fig. 11 β (left) and θ (right) parameters of the Ekman model used in the computation of the SURCOUF currents. Parameters are displayed by month (from 1 Jan to 12 Dec) and latitude (ranging between 10° S to 10° N). The units are (metres per second)/(Newtons per square metre) and degrees, respectively



were interpolated along the drifting buoy trajectories and subtracted from the buoy velocities. The residual ageostrophic current was further filtered using a 1.25- to 20-day band pass filter to focus on the frequencies where the coherency between the wind stress and the Ekman currents is maximal (Rio and Hernandez 2003). Then ERA INTERIM wind stress values were interpolated along the drifting buoy trajectories and also band-pass filtered. A least square fit was finally performed between \vec{u}_{ek} and $\vec{\tau}$ so as to obtain the β and θ parameters by latitudinal bands and by month. The resulting parameters are plotted in Fig. 11. For this specific study, the least square fit was performed on drifting buoy velocities available for the year 2006 in order to be independent from the analysis time period (2007–2008). Then Ekman currents were estimated and added to the geostrophic currents to obtain an estimate of the total surface current. Note that removing the drifters from our study period (July 2007 through December 2008) from the SURCOUF mean fields degraded the trajectory estimates in all cases. But the increase in trajectory error was similar to the half-width of the 95% confidence limits. For example, the 80th percentile for 3-day trajectories changed from 70 ± 3 to 73 ± 3 km in Table 4, while for 7-day trajectories changed from 145 ± 10 to 153 ± 10 km. In other words, the change was barely significant at the 95% level. This was to be expected because the AOML drifters from our study period and main analysis region were not the dominant determinant of the mean field there since less than 15%

of the 244,608 drifter velocity measurements within the main analysis region fell within the July 2007 to December 2008 time window.

References

- Barnier B, Madec G, Penduff T, Molines J-M, Treguier A-M, Le Sommer J, Beckmann A, Biastoch A, Böning C, Dengg J, Derval C, Durand, E, Gulev S, Remy E, Talandier C, Theetten S, Maltrud M, McClean J, De Cuevas B (2006) Impact of partial steps and momentum advection schemes in a global ocean circulation model at eddy-permitting resolution. *Ocean Dyn* 56:543–567
- Barnier B, Reynaud T, Beckmann A, Böning C, Molines J, Barnard S, Jia Y (2001) On the seasonal variability and eddies in the North Brazil Current: insights from model intercomparison experiments. *Prog Oceanogr* 48(2–3):195–230
- Barron CN, Kara AB, Martin PJ, Rhodes RC, Smedstad LF (2006) Formulation, implementation and examination of vertical coordinate choices in the global Navy Coastal Ocean Model (NCOM). *Ocean Model* 11:347–375
- Barron CN, Smedstad LF (2002) Global river inflow within the navy coastal ocean model. In: *Proceedings, MTS/IEEE oceans 2002 conference*. MTS/IEEE, Miloxi, MS, USA, pp 1472–1479
- Barron CN, Smedstad LF, Dastugue JM, Smedstad OM (2007) Evaluation of ocean models using observed and simulated drifter trajectories: impact of sea surface height on synthetic profiles for data assimilation. *J Geophys Res Oceans* 112(C07019). doi:10.1029/2006JC003982
- Benkiran M, Greiner E (2008) Impact of the incremental analysis updates on a real-time system of the North Atlantic Ocean. *J Atmos Ocean Technol* 25(11):2055–2073

- Berrisford P, Dee D, Fielding K, Fuentes M, Kallberg P, Kobayashi S, Uppala S (2009) The ERA-Interim archive. ERA report series 1, ECMWF, Shinfield Park, Reading, UK, p 16
- Blanke B, Delecluse P (1993) Variability of the tropical Atlantic-ocean simulated by a general-circulation model with 2 different mixed-layer physics. *J Phys Oceanogr* 23(7):1363–1388
- Bleck R (2002) An oceanic general circulation model framed in hybrid isopycnic-Cartesian coordinates. *Ocean Model* 37:55–88
- Bloom SC, Takacs LL, DaSilva AM, Levina D (1996) Data assimilation using incremental analysis updates. *Mon Weather Rev* 124(6):1256–1271
- Chassignet E, Hurlburt H, Smedstad O, Halliwell G, Hogan P, Wallcraft A, Bleck R (2006) Ocean prediction with the hybrid coordinate ocean model (HYCOM). In: Chassignet E, Verron J (eds) *Ocean weather forecasting*. Springer, Berlin, pp 413–426
- Chassignet EP, Hurlburt HE, Metzger EJ, Smedstad OM, Cummings JA, Halliwell GR, Bleck R, Baraille R, Wallcraft AJ, Lozano C, Tolman HL, Srinivasan A, Hankin S, Cornillon P, Weisberg R, Barth A, He R, Werner F, Wilkin J (2009) US GODAE: global ocean prediction with the hybrid coordinate ocean model (HYCOM). *Oceanography* 22(2, Sp. Iss. SI):64–75
- Chassignet EP, Smith LT, Halliwell GR, Bleck R (2003) North Atlantic simulations with the hybrid coordinate ocean model (HYCOM): impact of the vertical coordinate choice, reference pressure, and thermobaricity. *J Phys Oceanogr* 33:2504–2526
- Chelton DB, Schlax MG, Samelson RM, de Szoeke RA (2007) Global observations of large oceanic eddies. *Geophys Res Lett* 34:L15606. doi:10.1029/2007GL030812
- Cox M (1980) Generation and propagation of 30-day waves in a numerical model of the Pacific. *J Phys Oceanogr* 10:1168–1186
- Cummings JA (2005) Operational multivariate ocean data assimilation. *Q J R Met Soc* 131:3583–3604
- Cushman-Roisin B, Beckers J-M (2010) *Introduction to geophysical fluid dynamics physical and numerical aspects*, 2nd edn. Academic, London, p 875+ xiv
- Dai A, Trenberth KE (2002) Estimates of freshwater discharge from continents: latitudinal and seasonal variations. *J Hydrometeorol* 3:660–687
- Davidson FJM, Allen A, Brassington GB, Breivik O, Daniel P, Kamachi M, Sato S, King B, Lefevre F, Sutton M, Kaneko H (2009) Applications of GODAE ocean current forecasts to search and rescue and ship routing. *Oceanography* 22(3):176–181
- DRAKKAR Group (2007) Eddy-permitting ocean circulation hindcasts of past decades. *CLIVAR Exchanges* No 42. 12(3):8–10
- Drévillon M, Greiner E, Paradis D, Payan C, Lellouche JM, Refray G, Durand E, Law-Chune S, Cailleau S (2012) A strategy for producing refined currents in the equatorial Atlantic in the context of the search of the AF447 wreckage. *Ocean Dyn* (in press)
- Dutrieux P, Menkes CE, Vialard J, Flament P, Blanke B (2008) Lagrangian study of tropical instability vortices in the Atlantic. *J Phys Oceanogr* 38(2):400–417
- Efron B (1979) Bootstrap methods: another look at the jackknife. *Ann Stat* 7:1–26
- Ellipot S, Lumpkin R (2008) Spectral description of oceanic near-surface variability. *Geophys Res Lett* 35(L05606). doi:10.1029/2007GL032874
- Foltz G, Carton J, Chassignet E (2004) Tropical instability vortices in the Atlantic Ocean. *J Geophys Res Oceans* 109(C3):C03029. doi:10.1029/2003JC001942
- Fox D, Teague W, Barron C, Carnes M, Lee C (2002) The modular ocean data assimilation system (MODAS). *J Atmos Ocean Technol* 19:240–252
- Gentemann C, Minnett P, Sienkiewicz J, DeMaria M, Cummings J, Jin Y, Doyle J, Gramer L, Barron C, Casey K, Donlon C (2009) MISST: the multi-sensor improved sea surface temperature project. *Oceanography* 22(2, Sp. Iss. SI):76–87
- Goni G, Johns W (2001) A census of North Brazil Current rings observed from TOPEX/POSEIDON altimetry: 1992–1998. *Geophys Res Lett* 28(1):1–4
- Goosse H, Campin JM, Deleersnijder E, Fichefet T, Mathieu PP, Maqueda MAM, Tartinville B (2001) Description of the CLIO model version 3.0. Tech. rep., Institut d'Astronomie et de Géophysique Georges Lemaitre, Catholic University of Louvain, Belgium, p 49
- Griffa A, Piterbarg L, Özgökmen T (2004) Predictability of Lagrangian particle trajectories: effects of smoothing of the underlying Eulerian flow. *J Mar Res* 62(1):1–35
- Hackett B, Comerma E, Daniel P, Ichikawa H (2009) Marine oil pollution prediction. *Oceanography* 22(3):168–175
- Huntley HS, Lipphardt BL Jr, Kirwan AD Jr (2011) Lagrangian predictability assessed in the East China Sea. *Ocean Model* 36(1–2):163–178
- Jochum M, Malanotte-Rizzoli P, Busalacchi A (2004) Tropical instability waves in the Atlantic Ocean. *Ocean Model* 7(1–2):145–163
- Kennan S, Flament P (2000) Observations of a tropical instability vortex. *J Phys Oceanogr* 30(9):2277–2301
- LaCasce JH (2008) Statistics from lagrangian observations. Summer school on transport in geographical flows-Ten years after, Aosta, Italy, Jun, 2004. *Prog Oceanogr* 77(1):1–29
- LaCasce JH (2010) Relative displacement probability distribution functions from balloons and drifters. *J Mar Res* 68(3–4):433–457
- Large WG, McWilliams JC, Doney SC (1994) Oceanic vertical mixing—a review and a model with a nonlocal boundary layer parameterization. *Rev Geophys* 32:363–403
- Leith C (1974) Theoretical skill of Monte-Carlo forecasts. *Mon Weather Rev* 102(6):409–418
- Lumpkin R, Elipot S (2010) Surface drifter pair spreading in the North Atlantic. *J Geophys Res Oceans* 115:C12017
- Lumpkin R, Pazos M (2007) Measuring surface currents with surface velocity program drifters: the instrument, its data, and some recent results. In: Griffa A, Kirwan AD, Mariano A, Özgökmen T, Rossby T (eds) *Lagrangian analysis and prediction of coastal and ocean dynamics*. Cambridge University Press, Cambridge, pp 39–67
- Madec G (2008) NEMO ocean engine. Note du pole de modélisation, Institut Pierre-Simon Laplace (IPSL), France, No 27, p 322
- Mellor G, Yamada T (1974) Hierarchy of turbulence closure models for planetary boundary-layers. *J Atmos Sci* 31(7):1791–1806
- Menkes C, Kennan S, Flament P, Dandonneau Y, Masson S, Biessy B, Marchal E, Eldin G, Grelet J, Montel Y, Morliere A, Lebourges-Dhaussy A, Moulin C, Champalbert G, Herbland A (2002) A whirling ecosystem in the equatorial Atlantic. *Geophys Res Lett* 29(11):1553. doi:10.1029/2001GL014576
- Metzger E, Smedstad O, Thoppil P, Hurlburt H, Franklin D, Peggion G, Shriver J, Townsend T, Wallcraft A (2010) Validation test report for the global ocean forecast system

- v3.0—1/12° HYCOM/NCODA: phase II. NRL memo. Technical report NRL/MR/7320-10-9236, NRL
- Metzger E, Smedstad O, Thoppil P, Hurlburt H, Wallcraft A, Franklin D, Shriver J, Smedstad L (2008) Validation test report for the global ocean prediction system v3.0—1/12° HYCOM/NCODA: phase I. NRL memo. Technical report NRL/MR/7320-08-9148, NRL
- Murphy J (1988) The impact of ensemble forecasts on predictability. *Q J R Met Soc* 114(480):463–493
- Niiler PP, Sybrandy AS, Bi K, Poulain PM, Bitterman D (1995) Measurements of the water-following capability of holey-sock and TRISTAR drifters. *Deep-Sea Res I* 42(11–12):1951–1964
- Ollitrault M (2010) Determination of the search zone for phase 3 of the sea search operations for the airbus A330, flight AF447. Tech. rep., BEA: Bureau d'Enquetes et d'Analyses, Paris, France, p 3
- Ourmieres Y, Brankart JM, Berline L, Brasseur P, Verron J (2006) Incremental analysis update implementation into a sequential ocean data assimilation system. *J Atmos Ocean Technol* 23(12):1729–1744
- Özgökmen T, Griffa A, Mariano A, Piterbarg L (2000) On the predictability of lagrangian trajectories in the ocean. *J Atmos Ocean Technol* 17(3):366–383
- Özgökmen T, Piterbarg L, Mariano A, Ryan E (2001) Predictability of drifter trajectories in the tropical Pacific Ocean. *J Phys Oceanogr* 31:2691–2720
- Penduff T, Sommer JL, Barnier B, Treguier AM, Molines J-M, Madec G (2007) Influence of numerical schemes on current-topography interactions in 1/4° global ocean simulations. *Ocean Sci* 3:509–524
- Pham DT, Verron J, Roubaud MC (1998) A singular evolutive extended Kalman filter for data assimilation in oceanography. *J Mar Sys* 16:323–340
- Price J (1981) Upper ocean response to a hurricane. *J Phys Oceanogr* 11(2):153–175
- Price JF (1983) Internal wave wake of a moving storm. Part 1. Scales, energy budget and observations. *J Phys Oceanogr* 13(6):949–965
- Reynolds RW, Smith TM, Liu C, Chelton DB, Casey KS, Schlax MG (2007) Daily high-resolution blended analyses for sea surface temperature. *J Climate* 20:5473–5496
- Richardson LF (1926) Atmospheric diffusion on a distance-neighbour graph. In: *Proceedings of the royal society of London, series A*, vol 110
- Richardson P, Reverdin G (1987) Seasonal cycle of velocity in the atlantic north equatorial countercurrent as measured by surface drifters, current meters, and ship drifts. *J Geophys Res Oceans* 92(C4):3691–3708
- Rio MH, Guinehut S, Larnicol G (2011) New CNES-CLS09 global mean dynamic topography computed from the combination of GRACE data, altimetry, and in situ measurements. *J Geophys Res Oceans* 116:C07018. doi:10.1029/2010JC006505
- Rio MH, Hernandez F (2003) High-frequency response of wind-driven currents measured by drifting buoys and altimetry over the world ocean. *J Geophys Res Oceans* 108(C8):3283. doi:10.1029/2002JC001655
- Rio MH, Hernandez F (2004) A mean dynamic topography computed over the world ocean from altimetry, in-situ measurements and a geoid model. *J Geophys Res* 109(C12):C12032
- Rixen M, Book JW, Carta A, Grandi V, Gualdesi L, Stoner R, Ranelli P, Cavanna A, Zanasca P, Baldasserini G, Trangeled A, Lewis C, Trees C, Grasso R, Giannellini S, Fabiani A, Merani D, Berni A, Leonard M, Martin, P, Rowley C, Hulbert M, Quaid A, Goode W, Preller R, Pinardi N, Oddo P, Guarneri A, Chiggato J, Carniel S, Russo A, Tudor M, Lenartz F, Vandenbulcke L (2009) Improved ocean prediction skill and reduced uncertainty in the coastal region from multi-model super-ensembles. *J Mar Sys* 78(Sp. Iss. SI Suppl. S):S282–S289
- Rixen M, Ferreira-Coelho E (2007) Operational surface drift prediction using linear and non-linear hyper-ensemble statistics on atmospheric and ocean models. *J Mar Sys* 65(1–4):105–121
- Rixen M, Ferreira-Coelho E, Signell R (2008) Surface drift prediction in the Adriatic Sea using hyper-ensemble statistics on atmospheric, ocean and wave models: uncertainties and probability distribution areas. *J Mar Sys* 69(1–2):86–98
- Rosmond T, Teixeira J, Peng M, Hogan T, Pauley R (2002) Navy Operational Global Atmospheric Prediction System (NOGAPS): forcing for ocean models. *Oceanography* 15:99–108
- Sawford B (2001) Turbulent relative dispersion. *Ann Rev Fluid Mech* 33:289–317
- Tranchant B, Testut C-E, Renault L, Ferry N, Birol F, Brasseur P (2008) Expected impact of the future SMOS and Aquarius Ocean surface salinity missions in the Mercator Ocean operational systems: new perspectives to monitor ocean circulation. *Remote Sens Environ* 112(4):1476–1487
- Tulloch R, Marshall J, Smith KS (2009) Interpretation of the propagation of surface altimetric observations in terms of planetary waves and geostrophic turbulence. *J Geophys Res* 114:C02005. doi:10.1029/2008JC005055
- van Sebille E, van Leeuwen PJ, Biastoch A, Barron C, de Ruijter W (2009) Lagrangian validation of numerical drifter trajectories using drifting buoys: application to the Agulhas system. *Ocean Model* 29(4):269–276
- von Schuckmann K, Brandt P, Eden C (2008) Generation of tropical instability waves in the Atlantic Ocean. *J Geophys Res Oceans* 113(C8):C08034. doi:10.1029/2007JC004712
- Weisberg R, Hickman J, Tang T, Weingartner T (1987) Velocity and temperature observations during the seasonal response of the equatorial Atlantic experiment at 0N, 28W. *J Geophys Res* 92(C5):5061–5075
- Weisberg RH, Weingartner TJ (1988) Instability waves in the equatorial Atlantic. *J Phys Oceanogr* 18(11):1641–1657